Supplemental Material

Characterization and validation of tidally calibrated strains from the Alto Tiberina Near Fault Observatory Strainmeter Array (TABOO-NFO-STAR)

C. Hanagan[1], E. Mandler[2], R. A. Bennett[1], L. Chiaraluce[2], M. Gottlieb[3], A. Gualandi[2,4], A. Hughes[1], W. Johnson[3], D. Mencin[3], S. Marzorati[2]

[1]Department of Geosciences, The University of Arizona, Tucson, AZ, USA

[2]Istituto Nazionale di Geofisica e Vulcanologia, Rome, Italy

[3]EarthScope, USA

[4]Department of Earth Sciences, University of Cambridge, UK

Supporting Information

This document contains the supplementary text (A-B), figures (S1-S10) and tables (S1-S10) for the main article. The processing and calibration workflow presented here is now implemented in the Earthscopestraintools python package (Gottlieb and Hanagan, 2024; https://earthscopestraintools.readthedocs.io/en/latest/notebooks/TidalCalibrationEarthscopestraintools.html), which can guide future re-calibration as longer time spans of clean data become available. The raw data presented here are managed by EarthScope (UNAVCO) as part of the NOTA Borehole Seismic Network, available through web services (https://service.iris.edu/fdsnws/).

Supplemental Text A: Data processing and manufacturer's calibrations

We start with the 1 Hz raw strainmeter gauge data from the IRIS Data Management Center for the longest available time span without significant gaps, ranging from 138 to 252 days with no more

than 1 cumulative hour of missing data (Figure 3; Table S1). We convert the raw gauge counts to linear strain (e) through the equation:

$$e_t = \frac{G}{D}\left[\frac{R_t 1\times10^{-8}}{1-R_t 1\times10^{-8}} - \frac{R_0 1\times10^{-8}}{1-R_0 1\times10^{-8}}\right] \text{ (equation S1)}$$

Where R_0 and R_t are the reference and measured raw count values at initial and final times, respectively. The factor of 10^{-8} converts directly to units of microstrain. G (0.2 mm) is a factor that accounts for the gap between capacitance plates in each gauge, and D (8.7 cm) is the instrument diameter.

Offsets or pulses hinder accurate estimation of the tidal constituents and barometric pressure response for each gauge, and can be common with these instruments (Hodgkinson et al., 2013). Instrumental calibration pulses or missing data, flagged with 999999 values are linearly interpolated and passed through a causal minimum-phase FIR filter, then decimated to 5 minutes (Agnew and Hodgkinson, 2007). Offsets result from known geophysical signals, such as coseismic offsets and dynamic strains, or from unknown sources related to instrumental issues or near-gauge formation heterogeneities. Historically, offsets were manually flagged and corrected in the processed level 2b data from EarthScope. We instead correct for offsets using first differences on the data with preliminary estimates of the linear trend, barometric pressure, and tides removed to reduce consistent over- or under-correction. The trend is calculated following a process similar to that of MIDAS for GNSS time series velocity estimates (Median Interannual Difference Adjusted for Skewness; Blewitt et al., 2016), which is relatively insensitive to the presence of offsets. Slopes are calculated at pairs of points separated by roughly one tidal day (24.84 hr), and outliers beyond two standard deviations of the mean are removed from the slope calculations. The median of the remaining set of slopes is used to detrend the data. The collocated surface barometric pressure data

is included as auxiliary input to Baytap08, which calculates a linear pressure response coefficient during the estimation of the tidal amplitudes and phases (Table S3). Both the gauge strains and pressure data are decimated to hourly after applying a 5th order, 2-hour low pass Butterworth filter. Times for the flagged data that were previously interpolated are included as input for Baytap08 to ignore in the regression. The estimated amplitudes and phases for the O1, M2, P1, K1, N2, and S2 tidal constituents are passed to the hartid function of SPOTL (Agnew, 2012) to forward model tidal time series for each gauge. The gauge pressure response coefficients from Baytap08 are used to scale the barometric pressure, which are then linearly interpolated to 5 minutes. The preliminary tidal and pressure corrections are then removed from the original 5-minute linearized gauge strains. Additional details on the program inputs can be found in the main text and code found in the earthscopestraintools notebook (https://earthscopestraintools.readthedocs.io/en/latest/notebooks/TidalCalibrationEarthscopestraintools.html). Any corrections for the tides or pressure mentioned in later sections are implemented through the same process outlined here.

Offsets are calculated from first differences on the pre-corrected data above a variable cutoff per gauge. The cutoff is designed as 10 times the mean of 75% of the first differences, thus excluding outliers. The values range from ~1 to 15 nanostrain at all sites, indicating the generally clean nature of the data (Figure S1). TSM6 contains more unexplained offsets than any other station, and determining the origin of these offsets is beyond the goal of this study. The offsets are cumulatively summed through time and removed from the uncorrected, hourly decimated data for final retrieval of the tidal constituent amplitudes and phases in Baytap08. Initial tests with the Network of the Americas (NOTA) borehole strainmeter (BSM) instruments demonstrated at least comparable, if

not better, success using the presented method for preparing data for tidal analysis than by manually cleaning the data of solely large offsets.

We calibrate the Alto Tiberina Near Fault Observatory Strainmeter Array (TABOO-NFO-STAR) BSMs using both the standard manufacturer's calibrations and the tidal calibrations as described in the main text. Nominally, the manufacturer's calibrations account for the strainmeter, borehole, and grout coupling to rock formation strains and the individual gauge orientations. Each linear gauge responds to some combination of strain acting parallel as well as perpendicular to its orientation; therefore, strain at a single gauge (e) oriented at angle θ from the x-axis (east) can be recast as a linear combination of areal and engineering shear strains, with isotropic areal and shear coupling coefficients c and d (Hart et al., 1996):

$$e = 0.5[ce_A + de_D cos(2\theta) + de_S sin(2\theta)] \text{ (equation S2)}$$

The areal (e_A), differential shear (e_D), and engineering shear (e_S) strains are regionally defined in the east/north reference system as e_{EE}+e_{NN}, e_{EE}-e_{NN}, and 2e_{EN} (Figure 2). The orientation of the first gauge (θ_1) is inferred from an internal magnetometer reading at the surface, and compared with the value at depth post-install, though these measurements are subject to error (Hodgkinson et al., 2013; Roeloffs, 2010). Gladwin and Hart (1985) determined theoretical values of 1.5 and 3 for c and d, respectively, for the GTSM instruments. This assumes perfectly isotropic coupling with equal sensitivity on all gauges, presumed relative grout and rock formation strengths, and an absence of sensitivity to vertical strain. For all gauges, equation S2 can be expanded to matrix form:

$$\begin{bmatrix} e_0 \\ e_1 \\ e_2 \\ e_3 \end{bmatrix} = 0.5 \begin{bmatrix} c & dcos(2\theta_1) & dsin(2\theta_1) \\ c & dcos(2(\theta_1+60)) & dsin(2(\theta_1+60)) \\ c & dcos(2(\theta_1+120)) & dsin(2(\theta_1+120)) \\ c & dcos(2(\theta_1+150)) & dsin(2(\theta_1+150)) \end{bmatrix} \begin{bmatrix} e_A \\ e_D \\ e_S \end{bmatrix}$$ (equation S3)

Where the factor of 0.5 and coupling matrix are multiplied by the regional strains. The Moore-Penrose pseudoinverse of the coupling matrix is the calibration matrix, applied to the linearized gauge strains. These matrices are included in the metadata associated with the instruments, hosted on the EarthScope Consortium site (e.g. for TSM1 http://bsm.unavco.org/bsm/level2/tstartsm1bit2021/TSM1.README.txt).

Supplemental Text B: Mandler et al. (2024) tidal calibration

We compare the calibration strategy followed in this paper to the one proposed in Mandler et al. (2024). The latter consists of waveform modeling for a set of tidal constituents (i.e., O1, K1, M2, S2, M3), though the reconstructed tidal time-series are dominated by the O1 and M2 bands (Canitano et al., 2018). The approach followed in Mandler et al. (2024) is data driven and does not require any further information than the location, starting time, and sampling rate of the GTSM data. The approach also skips data linearization (equation S1), and therefore goes directly from raw data counts to strain. It starts by assuming a simple isotropic calibration model, for which a coupling coefficient common to the four gauges exists for both the areal strain and shear strain components, and progressively increases the model complexity as needed.

To calibrate the six GTSMs deployed in central Italy, we focus on the same period outlined in Table S1 and adopt the more complex cross-coupled model (Section 5 of Mandler et al., 2024), which allows for a higher degree of free parameters. A simplistic model with constrained coupling coefficients fails to fit at least one strain component (Pearson coefficient R < 80%), which is likely

due to a combination of the recent installation of these strainmeters, preventing a long enough timespan to fully separate the suite of tidal constituents (at least one year is recommended to separate the constituents used following this method), and to the non-isotropic conditions of the coupled bedrock-grout-strainmeter system. Prior to extraction of the tidal constituents from the data, we correct for a linear barometric pressure response, derived from the collocated sensors as in the main text.

Adopting a cross-coupled model, we satisfactorily reproduce the theoretical tidal waveforms modeled with Gotic2 (Matsumoto et al., 2001; Table S8), with the sole exception of TSM1 engineering strain. Overall poor results are obtained for TSM4 due to large chunks of missing data. The approach proposed in Mandler et al. (2024) requires at least six months of continuous data for a thorough tidal extraction. The resulting calibration matrices for the six GTSMs are reported in Table S8, and these matrices are the ones used to compare with the calibration results presented in this paper.

Supplemental Figures

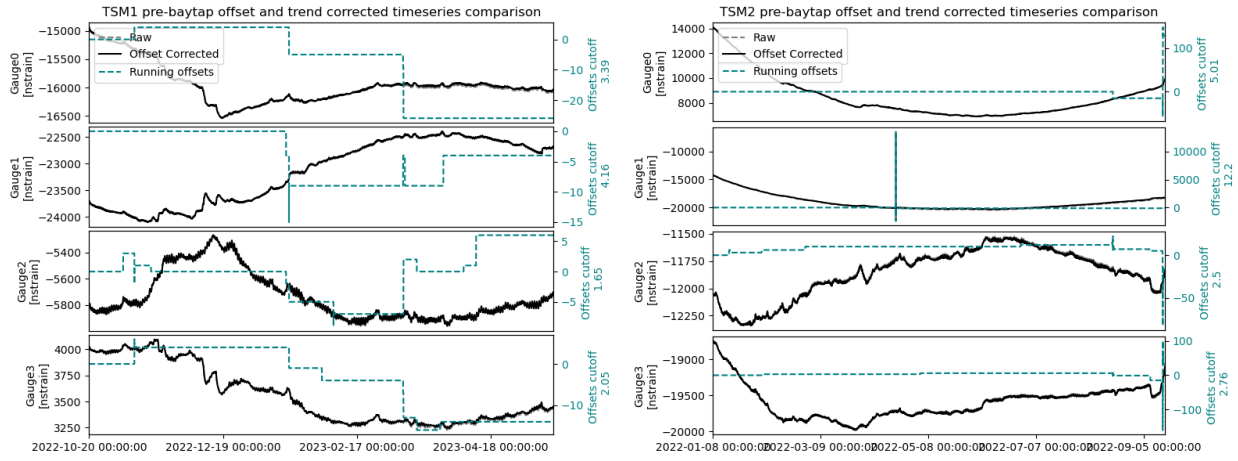

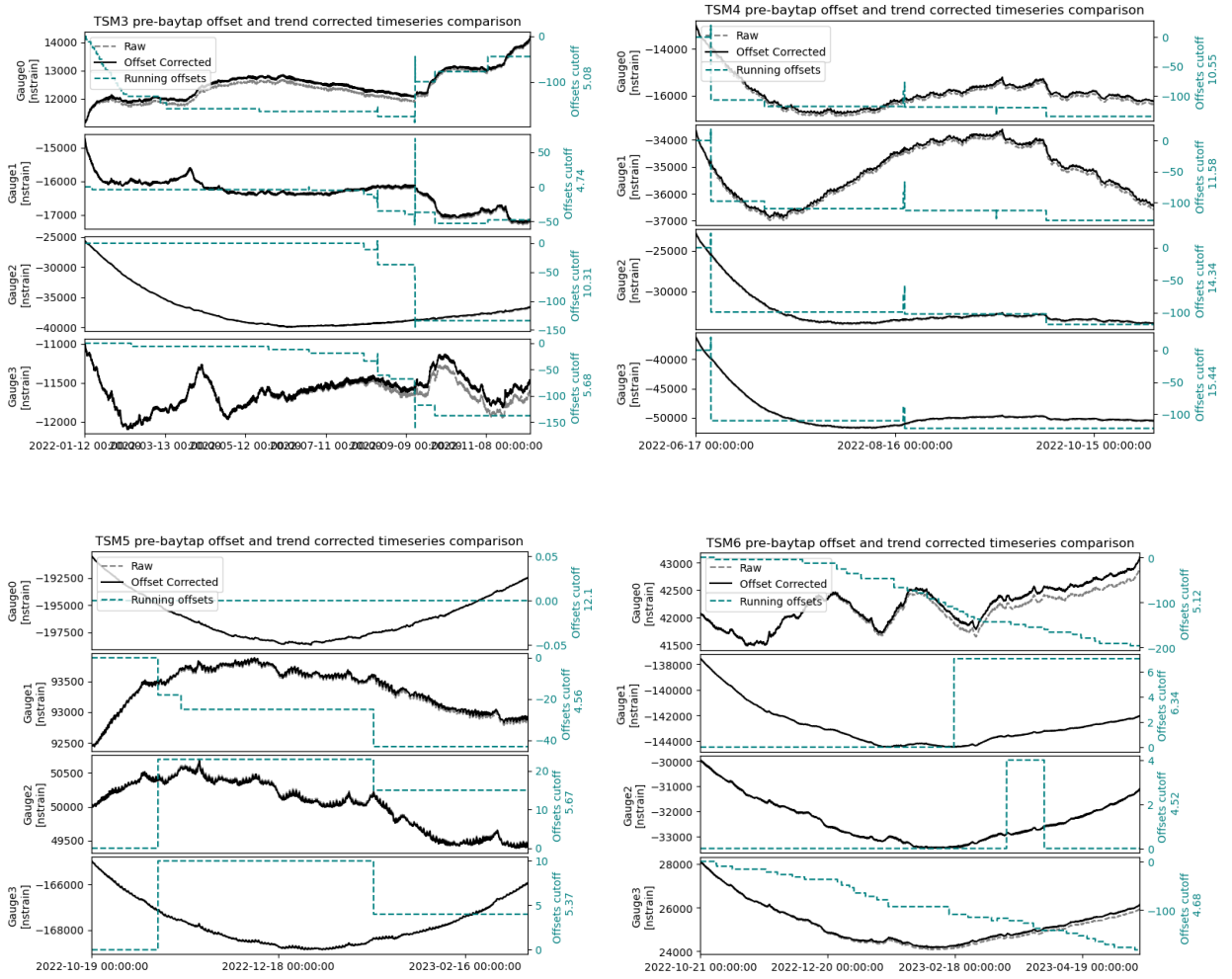

Figure S1. Offset corrected time series for the final Baytap08 tidal analysis presented in the methods section. Note that a linear trend and 999999-valued calibration pulses have been removed for visualization purposes, but are reinserted for the final Baytap08 run. For each subplot, strain is plotted in black, while the running cumulative offsets are plotted on separate y-axes in teal. The offset cutoff, determined as described in the main text, is likewise printed next to each secondary y-axis in teal.

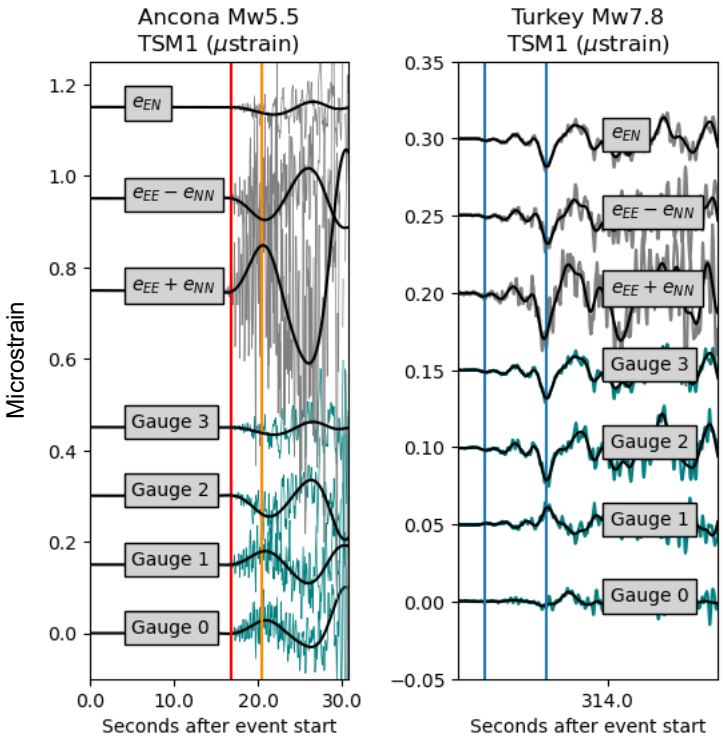

Figure S2. 20 Hz and 0.2 Hz lowpass filtered gauge and regional strains recorded at TSM1 from the Ancona Mw 5.5 thrust earthquake and the Turkey Mw 7.8 strike-slip earthquake. The red line marks the P-wave recorded on the collocated borehole seismometer, and the orange line marks the peak extensional strain associated with the low-frequency P wave pictured in Figure 7. The blue lines for the Kahramanmaras earthquake mark the peak extension associated with the low-frequency P and PP waves.

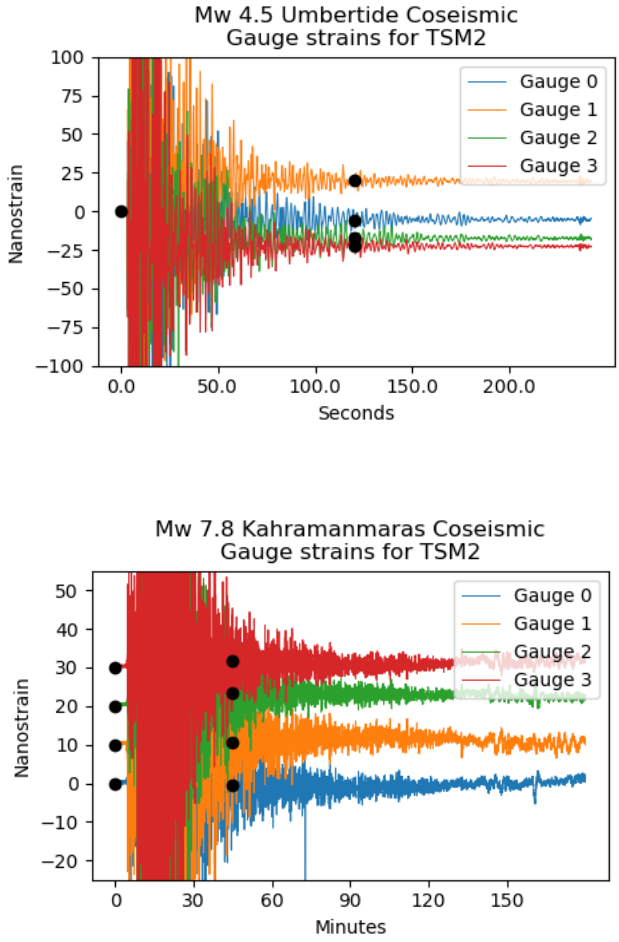

Figure S3. 20 Hz gauge strains recorded at TSM2 for the Mw 4.5 Umbertide mainshock and Mw 7.8 Kahramanmaras earthquake. Coseismic offsets are calculated as the difference between the second and first black point, with the second being calculated from the average strains spanning 1 to 2 minutes after the event start for Umbertide, and 30 to 60 minutes for Kahramanmaras.

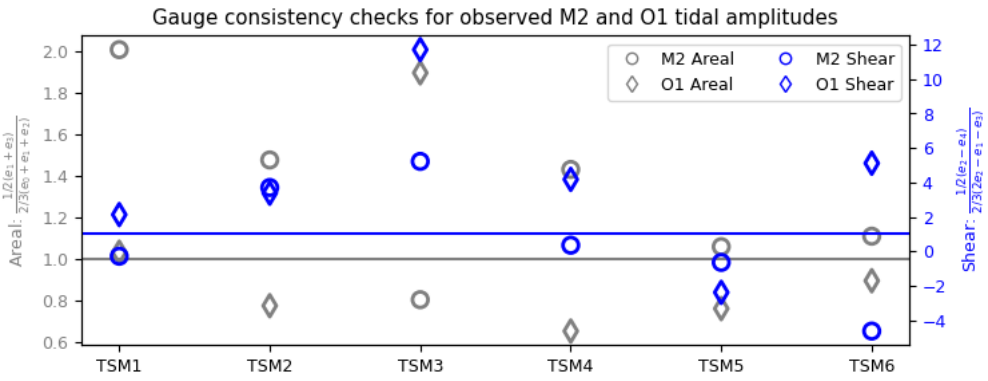

Figure S4. Gauge consistency calculations for the observed M2 and O1 tidal amplitudes. The results for the areal and shear strains are plotted on separate axes, colored grey and blue, respectively. The gray and blue horizontal lines for the amplitudes mark a value of 1, which would occur for isotropic conditions with equal gauge sensitivities.

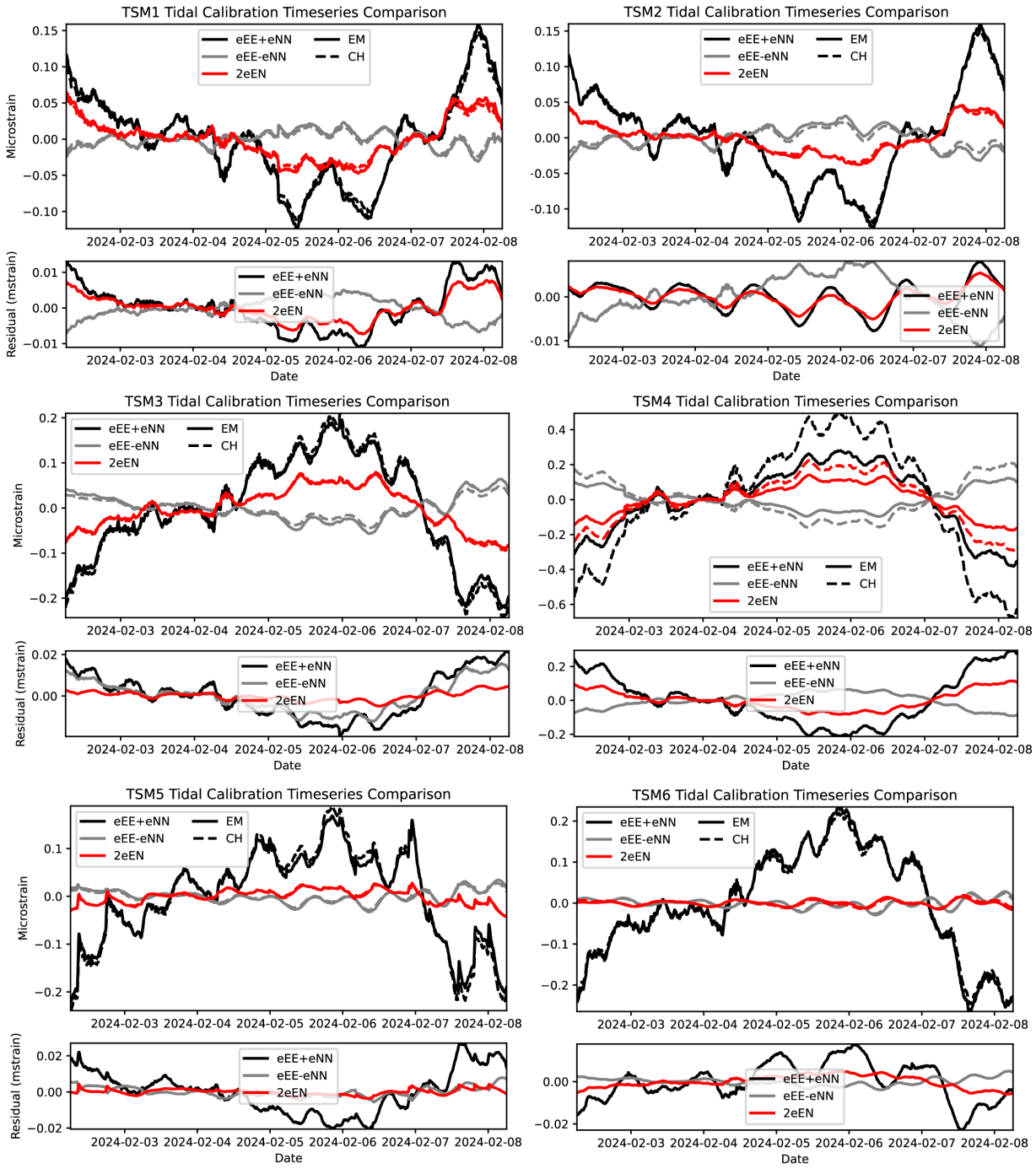

Figure S5. Time series comparison of regionally transformed strains from the calibration methodology presented in the main text (CH) and in Mandler et al. (2024; EM; Table S8). All strain components have been linearly detrended. The residuals are plotted below each station's panel as the EM calibrated time series subtracted from the CH calibrated time series. Overall, the

calibrated timeseries show good agreement. The only exception is TSM4, with differences up to 50% or more.

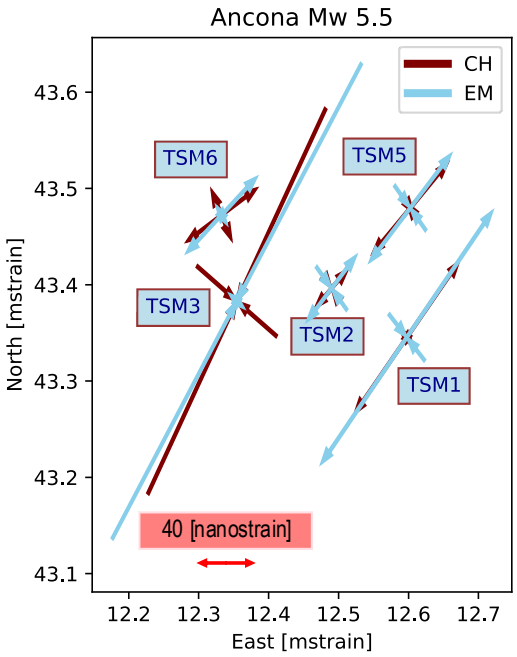

Figure S6. Comparison of coseismic offsets from the Mw5.5 Ancona thrust event for the STAR BSMs, excepting TSM4 which was not recording at the time. The results demonstrate close agreement between the calibrations presented here (CH) and from the approach described in Supplemental Text C and Mandler et al. (2024; EM) for short timespans.

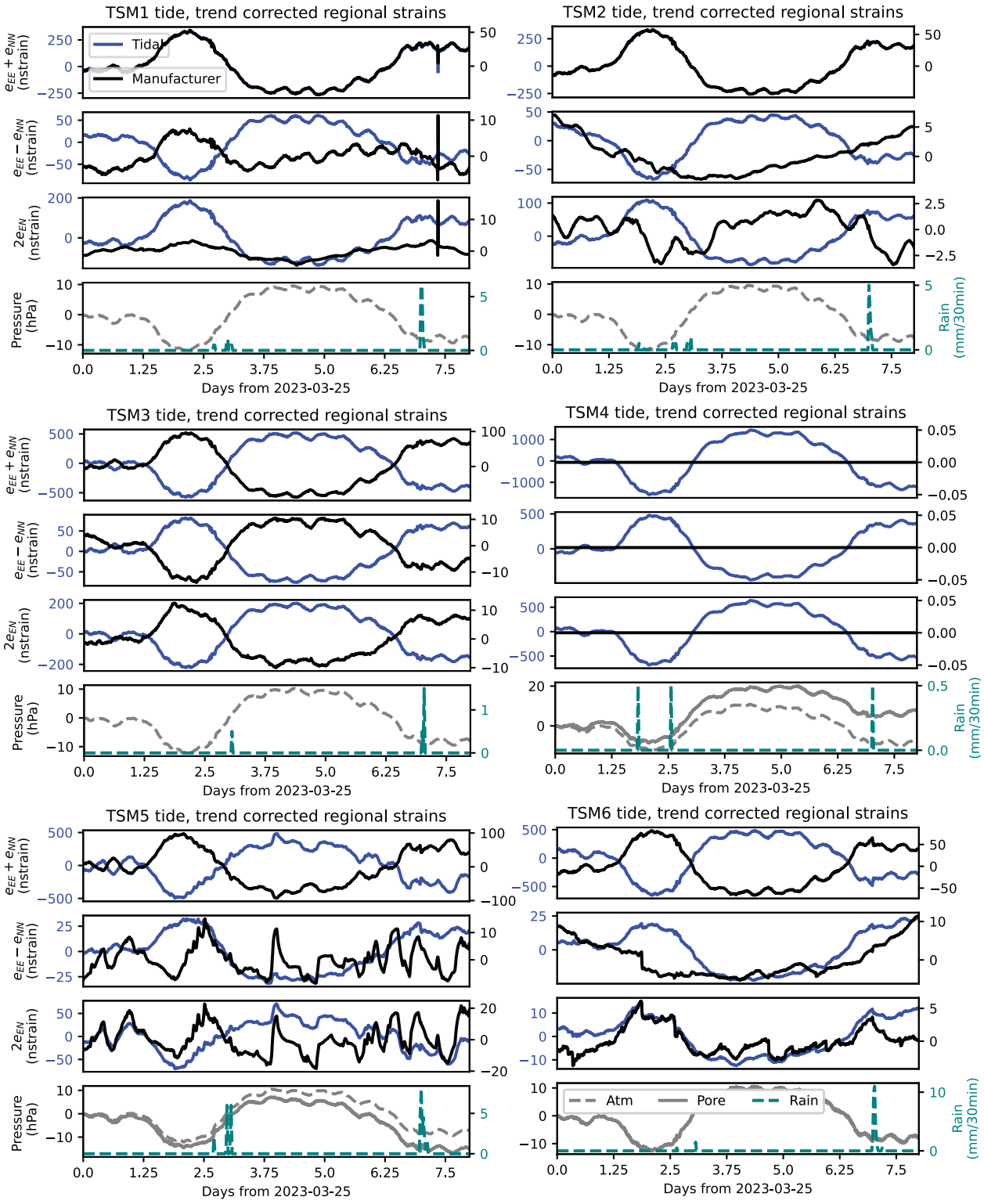

Figure S7. Comparison of the regionally transformed time series using the tidal (blue) and manufacturer's (black) calibrations over the course of a week. Barometric pressure (dashed grey)

and rainfall (dashed blue) are plotted for all stations, and pore pressure (solid grey) is available and plotted at TSM4-6. Both calibrations result in a similar areal strain pattern for TSM1 and TSM2 in the absence of overall negative areal coupling, but a reversed sign for TSM3 through TSM6 with negative overall areal coupling. The time series have been zeroed to the first value. Note the secondary vertical axis ticks for the manufacturer's calibrated strains and rainfall.

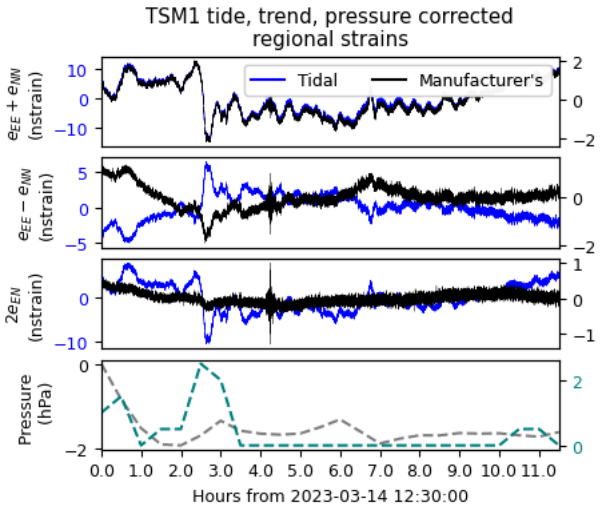
TSM1 tide, trend, pressure corrected
regional strains
Tidal
Manufacturer's
$e_{EE}+e_{NN}$ (nstrain)
$e_{EE}-e_{NN}$ (nstrain)
$2e_{EN}$ (nstrain)
Pressure (hPa)
Hours from 2023-03-14 12:30:00

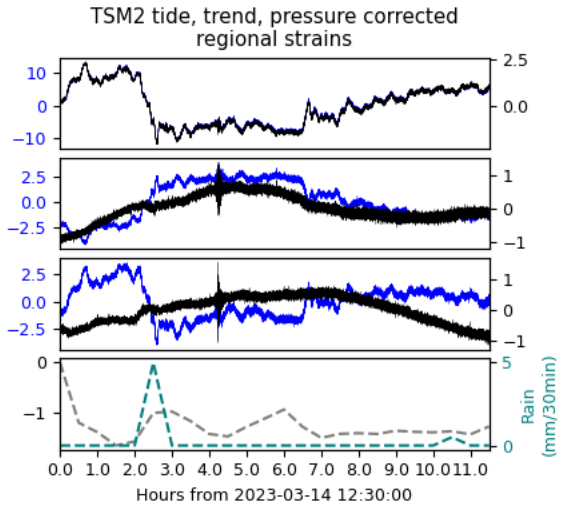
TSM2 tide, trend, pressure corrected
regional strains
Rain (mm/30min)
Hours from 2023-03-14 12:30:00

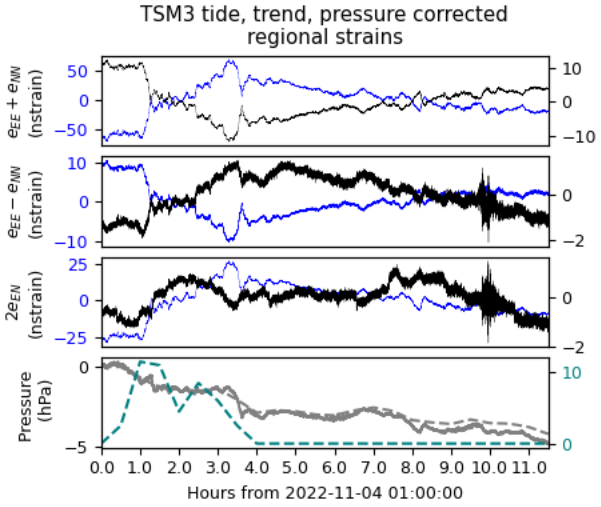
TSM3 tide, trend, pressure corrected
regional strains
$e_{EE}+e_{NN}$ (nstrain)
$e_{EE}-e_{NN}$ (nstrain)
$2e_{EN}$ (nstrain)
Pressure (hPa)
Hours from 2022-11-04 01:00:00

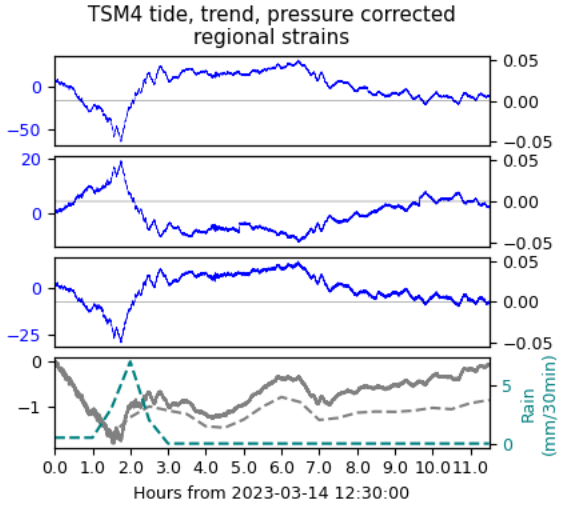
TSM4 tide, trend, pressure corrected
regional strains
Rain (mm/30min)
Hours from 2023-03-14 12:30:00

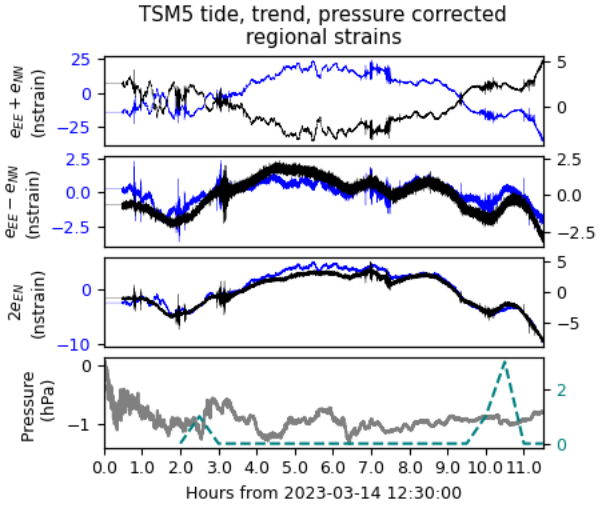
TSM5 tide, trend, pressure corrected
regional strains
$e_{EE}+e_{NN}$ (nstrain)
$e_{EE}-e_{NN}$ (nstrain)
$2e_{EN}$ (nstrain)
Pressure (hPa)
Hours from 2023-03-14 12:30:00

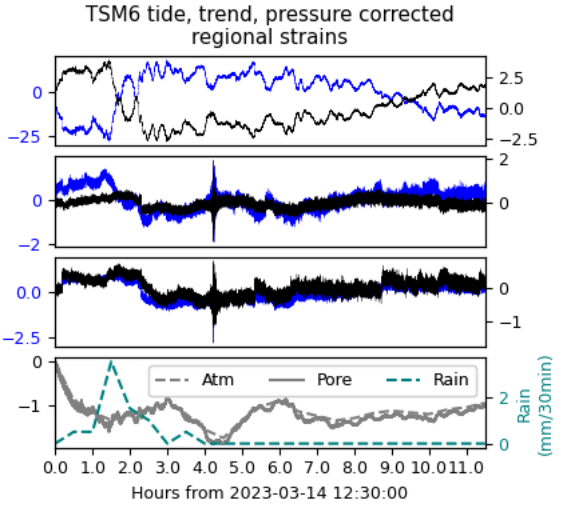
TSM6 tide, trend, pressure corrected
regional strains
Atm
Pore
Rain
Rain (mm/30min)
Hours from 2023-03-14 12:30:00

Figure S8. Regional strains calculated with the manufacturer's and tidal calibrations, demonstrating the response to rainfall for a half day. Data are corrected for a linear trend, tides, and barometric pressure response. TSM3 had no pore pressure data available on March 3rd, 2023, so we plot an example from October 28th, 2022, instead. Color coding is the same as in Figure S6.

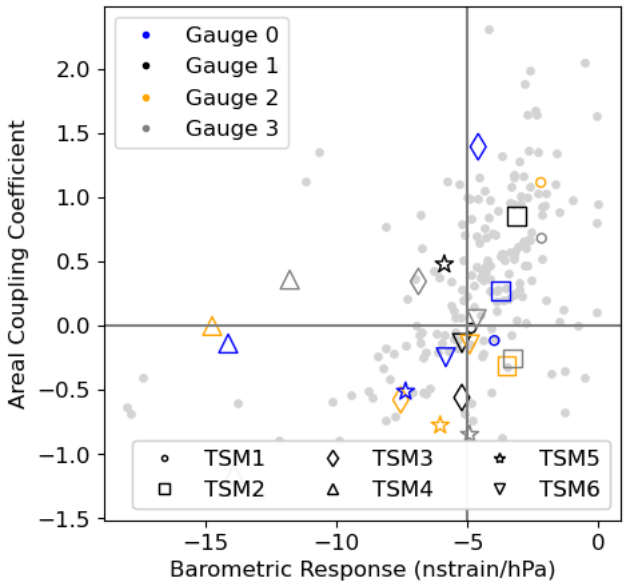

Figure S9. Areal coupling coefficients per gauge plotted against the BAYTAP08-estimated barometric pressure response. TSM1 and TSM2 have pressure response coefficient magnitudes of less than 5 nanostrain/hPa, and are the only stations with overall positive areal coupling. TSM3 through TSM6 are overall negatively coupled to areal strain, implying a higher degree of vertical coupling (Roeloffs, 2010). Light grey points in the background contain the results for NOTA BSMs from Hodgkinson et al. (2013).

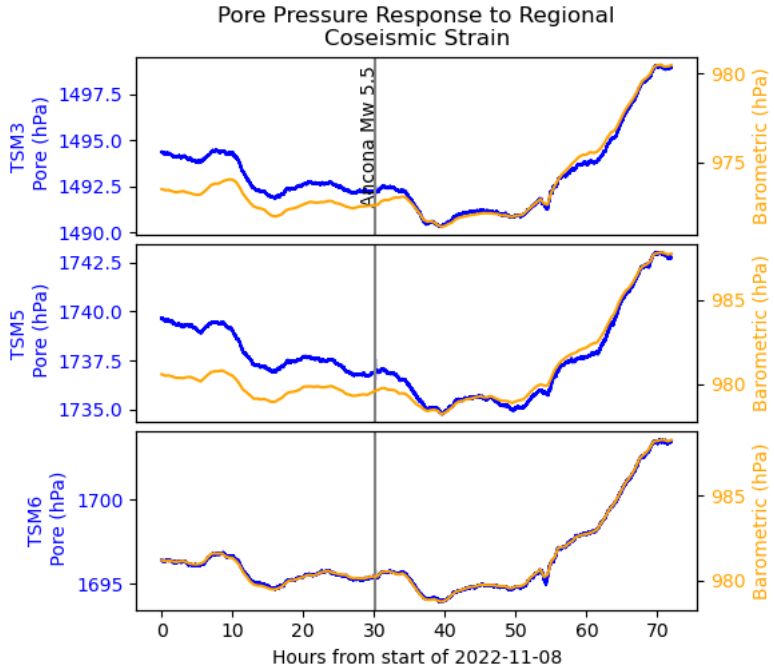
Pore Pressure Response to Regional Coseismic Strain
TSM3 Pore (hPa)
TSM5 Pore (hPa)
TSM6 Pore (hPa)
Barometric (hPa)
Ancona Mw 5.5
Hours from start of 2022-11-08

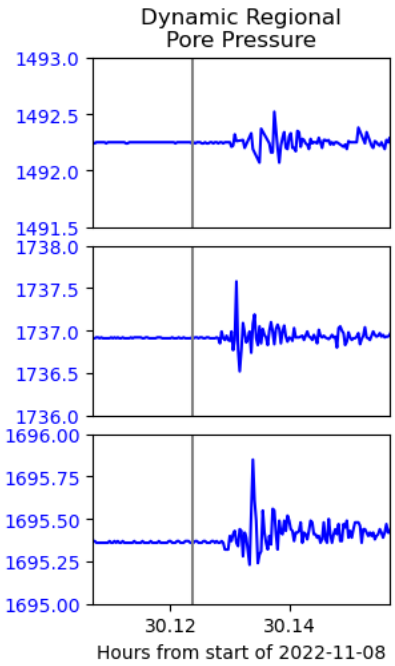
Dynamic Regional Pore Pressure
Hours from start of 2022-11-08

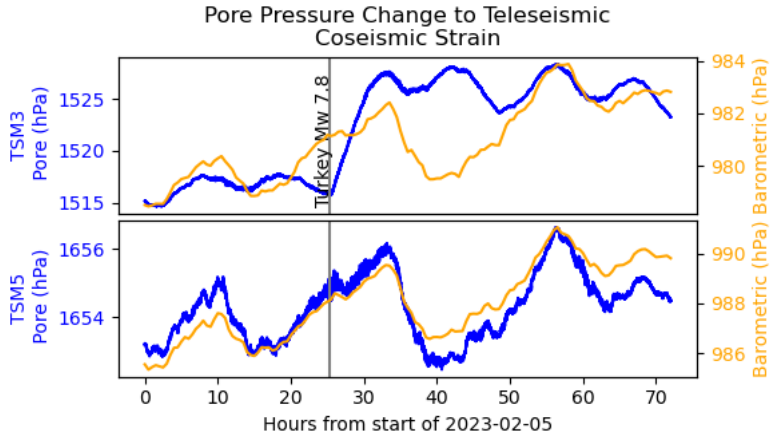
Pore Pressure Change to Teleseismic Coseismic Strain
TSM3 Pore (hPa)
TSM5 Pore (hPa)
Barometric (hPa)
Turkey Mw 7.8
Hours from start of 2023-02-05

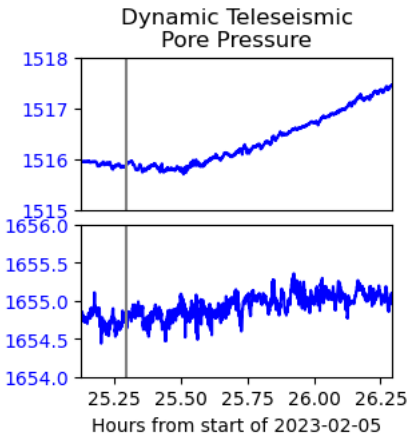
Dynamic Teleseismic Pore Pressure
Hours from start of 2023-02-05

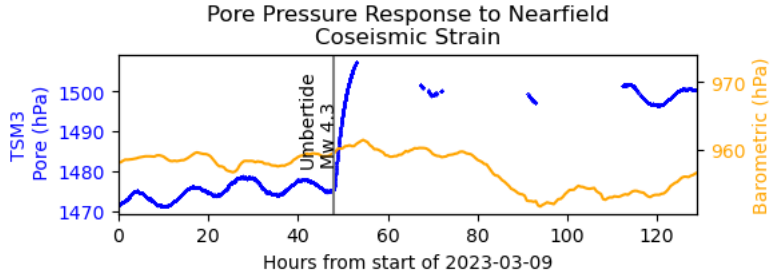
Pore Pressure Response to Nearfield Coseismic Strain
TSM3 Pore (hPa)
Barometric (hPa)
Umbertide Mw 4.3
Hours from start of 2023-03-09

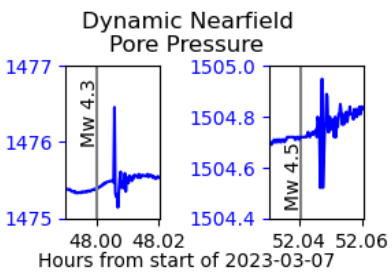
Dynamic Nearfield Pore Pressure
Mw 4.3
Mw 4.5
Hours from start of 2023-03-07

Figure S10. Pore pressure measured from transducers during the Mw 5.5 Ancona, Mw 7.8 Kahramanmaras, and Mw 4.3 and 4.5 Umbertide earthquakes. TSM3 transitions from a pore pressure response that tracks the barometric pressure in November 2022 during the Ancona event, toward a tidal response for the later 2023 events. TSM5 was also recording during the Umbertide sequence, but portrays no relevant additional information for our discussion, so we omit its record. Note that the barometric pressures and pore pressures are plotted on separate vertical axes. For each event, we zoom in on the dynamic pore pressure response in the right panels.

Supplemental Tables

Table S1. Station installation information and timeframes analyzed for the tidal calibration of each station.

Station	Start	End	Latitude (°)	Longitude (°)	Elevation (m)	Installation Azimuth (CH0 E of N in °)	Depth to Instrument (m)
TSM1	2022-10-20	2023-05-16	43.34536	12.597621	553	308	131.3
TSM2	2022-01-08	2022-09-17	43.39619	12.489944	630	345.4	158.1
TSM3	2022-01-12	2022-12-11	43.38298	12.354506	341	312.1	78.6
TSM4	2022-06-17	2022-11-02	43.3087	12.3046	270	Unknown	99.3
TSM5	2022-10-19	2023-03-08	43.479691	12.60252	379	342.9	116
TSM6	2022-10-21	2023-05-16	43.47246	12.33275	402	47.3	115.5

Table S2. Observed tidal amplitudes and phases from the Baytap08 (Tamura, 1991; Tamura and Agnew, 2008) analysis with associated 1-standard deviation uncertainty, and modeled amplitudes and phases using SPOTL (Agnew, 2012).

		M2		O1	
		Amplitude (nanostrain)	Phase (°)	Amplitude (nanostrain)	Phase (°)
TSM1					
Observed	Gauge 1	5.49 +- 0.06	-137.3 +- 0.6	1.66 +- 0.19	83 +- 6
	Gauge 2	6.41 +- 0.07	21.7 +- 0.6	1.8 +- 0.2	160 +- 8
	Gauge 3	8.60 +- 0.05	37.3 +- 0.3	7.6 +- 0.17	-25 +- 1
	Gauge 4	0.40 +- 0.05	-6.6 +- 7	5.3 +- 0.17	-12 +- 1.8
Modeled	EE+NN	15.41	5.83	11.46	0.42
	EE-NN	11.17	-160.57	2.87	1.57
	2EN	5.69	-81.02	3.69	94.07
TSM2					
Observed	Gauge 1	9.55 +- 0.07	28.1 +- 0.4	1.8 +- 0.2	-96 +- 7
	Gauge 2	1.51 +- 0.09	152 +- 3	7.3 +- 0.3	-14 +- 2.4
	Gauge 3	4.06 +- 0.05	-100.6 +- 0.6	3.7 +- 0.15	126 +- 2.3
	Gauge 4	5.32 +- 0.05	-2.3 +- 0.6	3.7 +- 0.17	159 +- 2.7
Modeled	EE+NN	15.38	5.85	11.46	0.42
	EE-NN	11.13	-160.95	2.87	1.31
	2EN	5.56	-80.75	3.67	93.97
TSM3					
Observed	Gauge 1	10.09 +- 0.2	63 +- 1.1	12.1 +- 0.6	-37 +- 2.7
	Gauge 2	14.7 +- 0.1	-149.1 +- 0.3	3.1 +- 0.3	107 +- 5
	Gauge 3	6.8 +- 0.2	19 +- 1.9	6.4 +- 0.6	-175 +- 5
	Gauge 4	11.49 +- 0.06	46.9 +- 0.3	4.5 +- 0.2	-83 +- 3
Modeled	EE+NN	15.38	5.87	11.46	0.39
	EE-NN	10.99	-161.80	2.87	0.91
	2EN	5.55	-80.98	3.67	94.00
TSM4					
Observed	Gauge 1	8.1 +- 0.19	-152 +- 1.3	0.9 +- 0.7	-27 +- 41
	Gauge 2	6.5 +- 0.3	-136 +- 2.5	7.9 +- 0.9	174 +- 7
	Gauge 3	3.6 +- 0.2	62 +- 3.0	3.0 +- 0.7	-101 +- 13
	Gauge 4	2.0 +- 0.17	155 +- 5	4.1 +- 0.6	-38 +- 9
Modeled	EE+NN	15.42	5.94	11.46	0.36
	EE-NN	10.93	-162.04	2.88	0.85
	2EN	5.66	-81.26	3.68	94.07
TSM5					
Observed	Gauge 1	14.3 +- 0.5	32 +- 2.0	7.4 +- 1.1	-168 +- 8
	Gauge 2	15.32 +- 0.07	163.2 +- 0.27	9.6 +- 0.26	-36 +- 1.6

	Gauge 3	16.9 +- 0.17	-129.0 +- 0.6	7.6 +- 0.5	115 +- 4
	Gauge 4	13.99 +- 0.07	-17.4 +- 0.3	11.9 +- 0.26	149 +- 1.2
Modeled	EE+NN	15.34	5.69	11.46	0.46
	EE-NN	11.28	-160.16	2.87	1.84
	2EN	5.46	-80.37	3.65	93.91
TSM6					
Observed	Gauge 1	6.02 +- 0.05	-45.5 +- 0.5	4.5 +- 0.19	134 +- 2.4
	Gauge 2	8.63 +- 0.05	63.5 +- 0.3	4.6 +- 0.17	-118 +- 2.12
	Gauge 3	13.15 +- 0.04	-165.8 +- 0.19	2.5 +- 0.16	13 +- 4
	Gauge 4	8.07 +- 0.05	-119.8 +- 0.4	4.0 +- 0.18	68 +- 2.6
Modeled	EE+NN	15.34	5.69	11.46	0.46
	EE-NN	11.28	-160.16	2.87	1.84
	2EN	5.46	-80.37	3.65	93.91

Table S3. Barometric pressure coefficients for each station from the BAYTAP08 analysis with associated 1-standard deviation uncertainty.

Barometric Pressure Response (hPa/nstrain)	TSM1	TSM2	TSM3	TSM4	TSM5	TSM6
Gauge 0	-3.98 +- 0.04	-3.72 +- 0.05	-4.6 +- 0.1	-14.1 +- 0.15	-7.4 +- 0.3	-5.83 +- 0.05
Gauge 1	-4.86 +- 0.05	-3.15 +- 0.06	-5.22 +- 0.06	-13.9 +- 0.15	-5.89 +- 0.05	-5.21 +- 0.04
Gauge 2	-2.20 +- 0.03	-3.52 +- 0.03	-7.6 +- 0.15	-14.8 +- 0.15	-6.05 +- 0.11	-4.92 +- 0.04
Gauge 3	-2.17 +- 0.03	-3.30 +- 0.03	-6.88 +- 0.06	-11.8 +- 0.14	-4.92 +- 0.06	-4.66 +- 0.05

Table S4. Earthquake information and source parameters (Scognamiglio et al., 2006; Dziewonski et al., 1981; Ekström et al., 2012).

Event	Time	Lat (°)	Lon (°)	Depth (km)	Strike (°)	Dip (°)	Rake (°)	Length (km)	Width (km)	Slip (cm)
Ancona Mw 5.5	2022-11-09 06:07:25.00	43.9833	13.3237	5	316	57	94	7.161	6.095	16.21
Kahramanmaras Mw 7.8	2023-02-06 01:17:36.50	37.2052	37.0401	22.9	228	89	-1	86.30	38.91	594.1
Umbertide Mw 4.3	2023-03-09 15:05:41.87	43.2892	12.3883	3	132	54	-103	1.954	2.317	2.48
Umbertide Mw 4.5	2023-03-09 19:08:06.78	43.2863	12.3905	3.3	142	52	-92	2.427	2.723	3.39

Table S5. Tidal calibration RMSE results for each station (equation 6). Note that the RMSE results per gauge contain real and imaginary parts, so we do not specify a unit. The amplitude and phase RMSE have been recombined and recalculated to original units of nanostrain (for amplitude) and degrees (for phase).

RMSE	TSM1	TSM2	TSM3	TSM4	TSM5	TSM6
Gauge 1	0.02	0.17	0.44	0.62	0.00	0.27
Gauge 2	0.34	0.02	0.07	0.91	0.42	0.01
Gauge 3	0.06	0.12	0.46	0.53	0.04	0.39
Gauge 4	0.19	0.10	0.16	0.52	0.23	0.03
Overall	0.20	0.12	0.33	0.67	0.24	0.24
Amplitude (nanostrain)	0.36	0.07	0.37	1.31	0.14	0.11
Phase (degree)	7.49	2.49	3.07	16.55	2.55	3.89

Table S6. Weighted calibration matrices for each station as described in the main text, with associated calibration RMSE. The preferred calibrations, without prior weights in the inversion, are presented in the main text Table 1.

	Component	Calibration Matrix				RMSE
TSM1	Areal	2.61	3.43	0.65	2.44	
	Differential	-0.24	-1.87	-0.05	-0.03	
	Engineering	2.05	2.04	-0.52	1.27	0.23
TSM2	Areal	1.45	2.94	1.70	1.55	
	Differential	-0.86	0.10	-0.01	-0.60	
	Engineering	-0.13	0.74	1.32	0.74	0.13
TSM3	Areal	0.11	-3.63	-1.38	-2.80	
	Differential	0.24	0.98	-0.21	0.27	
	Engineering	-0.34	-1.17	-0.43	-1.21	0.37
TSM4	Areal	-1.18	-2.10	-3.32	-1.39	
	Differential	1.21	0.13	0.29	0.82	
	Engineering	-0.17	-0.29	-2.06	-0.92	0.77
TSM5	Areal	-2.22	-1.76	-1.89	-0.27	
	Differential	-0.10	0.26	0.36	-0.13	
	Engineering	-0.46	-0.37	0.00	0.08	0.28
TSM6	Areal	-4.17	-2.73	-3.73	1.05	
	Differential	-0.27	-0.17	0.63	0.17	
	Engineering	0.33	-0.32	-0.15	0.28	0.28

Table S7. Theoretical calibration coupling coefficients for the STAR BSMs derived from the tidal calibrations in this study (Table 1) assuming accurate installation orientations. Numbers correspond to individual areal, differential, and shear coupling coefficients (in rows) for each gauge (in columns), consistent with the structure of the calibration matrices presented in table 1. TSM4 has no recorded installation orientation, so it is omitted.

TSM1	-0.1154 -0.0192 1.1158 0.6810 2.7660 -1.6310 -0.1933 -1.2338 -0.8861 0.0770 -6.1320 0.6460
TSM2	0.2734 0.8553 -0.3076 -0.2535 1.4461 1.6477 -12.9998 1.5171 1.6219 1.8767 1.5320 1.6192
TSM3	1.3937 -0.5596 -0.5773 0.3446 8.8073 2.1141 2.2417 1.4563 3.6264 2.6293 0.3130 3.9033
TSM5	-0.5120 0.4785 -0.7753 -0.8478 3.7411 3.4679 -16.6829 3.7860 1.3381 8.1797 3.8014 8.3957
TSM6	-0.2462 -0.1354 -0.1460 0.0515 -12.1257 1.2472 2.6690 1.1233 2.0446 5.1540 0.1284 4.6644

Table S8. Calibration matrices and Pearson correlation coefficients for the STAR BMSs calibrated following Mandler et al. (2024; see Supplementary text B). These calibrations are directly applied to the unlinearized, raw data counts to obtain units of strain.

TSM1			
	Areal Strain (EE+NN)	Differential Strain (EE-NN)	Engineering Shear Strain (2EN)
CALIBRATION MATRIX	0.1510 0.1746 0.0338 0.1169	-0.0146 -0.0977 -0.0053 0.0030	0.1114 0.0995 -0.0213 0.0606
R (Pearson coeff.)	89.80%	94.50%	76.90%

TSM2			
	Areal Strain (EE+NN)	Differential Strain (EE-NN)	Engineering Shear Strain (2EN)
CALIBRATION MATRIX	0.0725 0.1617 0.0807 0.0862	-0.0472 -0.0087 -0.0089 -0.0417	-0.0081 0.0442 0.0654 0.0394
R (Pearson coeff.)	95.60%	99.10%	96.80%
TSM3			
	Areal Strain (EE+NN)	Differential Strain (EE-NN)	Engineering Shear Strain (2EN)
CALIBRATION MATRIX	-0.0117 -0.1502 -0.0919 -0.0931	0.0207 0.0555 -0.0022 0.0133	-0.0233 -0.0484 -0.0307 -0.0442
R (Pearson coeff.)	96.20%	99.20%	93.80%
TSM4			
	Areal Strain (EE+NN)	Differential Strain (EE-NN)	Engineering Shear Strain (2EN)
CALIBRATION MATRIX	-0.0391 -0.0633 -0.0363 -0.0182	0.0546 -0.0075 -0.0256 0.0284	0.0007 0.0028 -0.0486 -0.0269
R (Pearson coeff.)	89.50%	91.80%	85.50%
TSM5			
	Areal Strain (EE+NN)	Differential Strain (EE-NN)	Engineering Shear Strain (2EN)
CALIBRATION MATRIX	-0.0858 -0.0686 -0.1037 0.0133	0.0011 0.0162 0.0247 -0.0097	-0.0206 -0.0145 -0.0029 0.0093
R (Pearson coeff.)	98.10%	99.40%	98.50%
TSM6			
	Areal Strain (EE+NN)	Differential Strain (EE-NN)	Engineering Shear Strain (2EN)
CALIBRATION MATRIX	-0.2583 -0.1253 -0.1865 0.0604	-0.0151 -0.0038 0.0372 0.0063	0.0151 -0.0201 -0.0106 0.0135
R (Pearson coeff.)	95.30%	99.40%	99.30%

Table S9. Dynamic strain analysis results for the axes of maximum horizontal strain associated with the Mw 5.5. Ancona low frequency P wave, and the Mw 7.8 Kahramanmaras P and PP waves. The time, strain magnitude, and azimuth misfit are calculated from the maximum principal axis.

Ancona Mw 5.5 P wave					
Station	Distance (km)	Time (s)	Velocity (km/s)	Amplitude (nstrain)	Azimuth Misfit (°)
TSM1	91.9	20.8	4.43	112.4	5.5
TSM2	93.7	21.5	4.36	68.7	5.0
TSM3	102.7	23.3	4.40	66.7	5.6
TSM5	80.7	19.7	4.09	68.6	4.6
TSM6	98.0	23.0	4.27	90.5	8.9
Kahramanmaras Mw 7.8 P wave					
TSM1	2175.4	273.5	7.96	-1.6	4.7
TSM2	2184.9	274.8	7.95	-1.4	9.6
TSM3	2195.5	276.4	7.94	-1.2	0.6
TSM5	2177.6	273.8	7.95	-1.7	0.6
TSM6	2198.9	277.0	7.94	-0.7	5.6
Kahramanmaras Mw 7.8 PP wave					
TSM1	2175.4	293.5	7.41	-23.0	3
TSM2	2184.9	294.8	7.41	-27.1	12
TSM3	2195.5	296.8	7.40	-25.2	8
TSM5	2177.6	293.8	7.41	-27.3	1
TSM6	2198.9	297.7	7.39	-18.3	7

Table S10. Observed static coseismic strain offsets for the tidally calibrated, manufacturer's calibrated, and modeled strains. The mean squared error for all components is reported between the tidal and manufacturer's calibrations versus the modeled strains. The directional misfit between the principal strain axes is also reported.

	Observed, Tide calibration (nanostrain)			Observed, Manufacturer's calibration (nanostrain)			Modeled (nanostrain)			MSE (nanostrain)		Directional Misfit (°)	
	E	N	EN	E	N	EN	E	N	EN	Tide-Model	Manufacturer's-Model	Tide-Model	Manufacturer's-Model
Ancona Mw 5.5													
TSM1	11.7	12.8	9.5	2	0.2	-1.5	0.7	1.7	2.3	98.7	6	4.1	9.4
TSM2	2.8	1.4	4.1	0.6	-0.2	1.8	1.3	1	2.2	2	0.7	2.8	5.1
TSM3	-23.2	-37.6	-15.3	9.2	6.9	-2.9	1.2	0.5	1.6	779.7	41.9	18.7	17.1
TSM5	8.8	7.1	6.5	-4.5	-0.3	7.5	2	1.6	3.5	28.2	20.7	1.8	9.7
TSM6	10.3	7.3	2.4	1.0	-3.5	0.9	1.7	0.2	1.7	41.3	4.8	4	21.5
Turkey Mw 7.8													
TSM1	10.5	18.3	10.9	3.2	0.1	-0.70	-0.30	-0.2	0.3	189.1	4.6	1.4	25
TSM2	3.7	5.4	2.5	0.7	0.8	0.5	-0.3	-0.2	0.3	17.4	0.7	1	7.1
TSM3	-14.5	-22.4	-10.3	5.7	5.1	-2.6	-0.3	-0.2	0.3	269.1	24.2	2.1	4.9
TSM5	4.4	5.3	1.0	-1.6	-0.8	0.5	-0.3	-0.2	0.3	17.5	0.7	4	13.6
TSM6	-1.3	-2.5	0.9	0.8	-0.6	0.3	-0.3	-0.2	0.3	2.2	0.5	25.9	40.1
Umbertide Mw 4.3													
TSM1	-6.4	2.8	-2.1	0.7	-0.2	1.9	-6	2	-2.3	0.3	22.2	2.9	23.2
TSM2	1.3	-4.8	-6.5	1.5	-1.5	-3.3	0.5	-8.1	-7.9	4.3	21.6	1.8	2
TSM3	-2.4	-29.2	-2.6	12.9	-4.0	2.5	2.1	-0.1	6.5	317.8	49	44.3	32.1
TSM6	0.7	-2	0.8	1.1	-1.3	0	0.6	-0.5	1	0.8	0.6	15.2	30.2
Umbertide Mw 4.5													
TSM1	-16.3	-5.1	-13.9	-1.7	2.2	4.80	-11.7	3.6	-5.3	57.1	67.5	16.7	38.8
TSM2	2.8	-18.4	-12	4.1	-5.6	-5.6	2.8	-15.1	-13.1	3.9	49.4	3.5	3.3
TSM3	7.4	-6.6	11.7	3.4	-9.8	10	1.5	7.8	8.9	83.7	104.7	25.4	26.5
TSM6	1.6	-1.2	1.6	1.4	-1.8	0.6	0.9	-0.3	1.7	0.4	1.2	10.1	25.3

References

Agnew, D. C., & Hodgkinson, K. (2007). Designing compact causal digital filters for low-frequency strainmeter data. Bulletin of the Seismological Society of America, 97(1B), 91-99. https://doi.org/10.1785/0120060088

Agnew, D. C. (2012). SPOTL: Some Programs for Ocean-Tide Loading. UC San Diego: Scripps Institution of Oceanography. Retrieved from https://escholarship.org/uc/item/954322pg

Blewitt, G., Kreemer, C., Hammond, W. C., and Gazeaux, J. (2016), MIDAS robust trend estimator for accurate GPS station velocities without step detection, J. Geophys. Res. Solid Earth, 121, 2054– 2068, doi:10.1002/2015JB012552.

Canitano, A., Hsu, YJ., Lee, HM. et al. Calibration for the shear strain of 3-component borehole strainmeters in eastern Taiwan through Earth and ocean tidal waveform modeling. J Geod 92, 223–240 (2018). doi:10.1007/s00190-017-1056-4

Dziewonski, A. M., T.-A. Chou and J. H. Woodhouse, Determination of earthquake source parameters from waveform data for studies of global and regional seismicity, J. Geophys. Res., 86, 2825-2852, 1981. doi:10.1029/JB086iB04p02825

Ekström, G., M. Nettles, and A. M. Dziewonski, The global CMT project 2004-2010: Centroid-moment tensors for 13,017 earthquakes, Phys. Earth Planet. Inter., 200-201, 1-9, 2012. doi:10.1016/j.pepi.2012.04.002

Gottlieb, M., & Hanagan, C., (2024). EarthScope/earthscopestraintools: v0.1.42 (V0.1.42-beta). Zenodo. https://doi.org/10.5281/zenodo.12193840

Gladwin, M. T., and R. Hart (1985), Design Parameters for Borehole Strain Instrumentation, Pure and Applied Geophysics, 123(1), 59–80, DOI:10.1007/BF00877049.

Hart, R. H. G., M. T. Gladwin, R. L. Gwyther, D. C. Agnew, and F. K. Wyatt (1996), Tidal calibration of borehole strain meters: Removing the effects of small-scale inhomogeneity, J. Geophys. Res., 101(B11), 25,553–25,571, doi:10.1029/96JB02273.

Hodgkinson, K., J. Langbein, B. Henderson, D. Mencin, and A. Borsa (2013), Tidal calibration of plate boundary observatory borehole strainmeters, J. Geophys. Res. Solid Earth, 118, 447–458, doi:10.1029/2012JB009651.

Mandler, E., Canitano, A., Belardinelli, M.E. *et al.* Tidal Calibration of the Gladwin Tensor Strain Monitor (GTSM) Array in Taiwan. *Pure Appl. Geophys.* (2024). https://doi.org/10.1007/s00024-024-03453-9

Matsumoto, K., Sato, T., Takanezawa, T., & Ooe, M. (2001). GOTIC2: A program for computation of oceanic tidal loading effect. *Journal of the Geodetic Society of Japan*, *47*(1), 243-248. https://doi.org/10.11366/sokuchi1954.47.243

Roeloffs, E. (2010), Tidal calibration of Plate Boundary Observatory borehole strainmeters: Roles of vertical and shear coupling, *J. Geophys. Res.*, 115, B06405, doi:10.1029/2009JB006407.

Scognamiglio, L., Tinti, E., Quintiliani, M. (2006). Time Domain Moment Tensor (TDMT) [Data set]. Istituto Nazionale di Geofisica e Vulcanologia (INGV). https://doi.org/10.13127/TDMT

Tamura, Y., & Agnew, D. C. (2008). Baytap08 User's Manual. UC San Diego: Scripps Institution of Oceanography. Retrieved from https://escholarship.org/uc/item/4c27740c

Tamura Y. and others, A procedure for tidal analysis with a Bayesian information criterion, Geophysical Journal International, Volume 104, Issue 3, March 1991, Pages 507–516, https://doi.org/10.1111/j.1365-246X.1991.tb05697.x